

# Collective tunneling of a Wigner necklace in carbon nanotubes

Dominik Szombathy,<sup>1,2,3</sup> Miklós Antal Werner,<sup>2,4</sup> Cătălin Pașcu Moca,<sup>5,6</sup>  
Örs Legeza,<sup>4,7</sup> Assaf Hamo,<sup>8</sup> Shahal Ilani,<sup>9</sup> and Gergely Zaránd<sup>5</sup>

<sup>1</sup>*Department of Theoretical Physics, Institute of Physics,  
Budapest University of Technology and Economics, Budafoki út 8., H-1111 Budapest, Hungary*

<sup>2</sup>*MTA-BME Quantum Dynamics and Correlations Research Group, Institute of Physics,  
Budapest University of Technology and Economics, Budafoki út 8., H-1111 Budapest, Hungary*

<sup>3</sup>*Nokia Bell Labs, Nokia Solutions and Networks Kft,  
1083 Budapest, Bókay János u. 36-42, Hungary*

<sup>4</sup>*Strongly Correlated Systems 'Lendület' Research Group,  
Wigner Research Centre for Physics, P.O. Box 49, 1525 Budapest, Hungary*

<sup>5</sup>*MTA-BME Quantum Dynamics and Correlations Research Group,  
Budapest University of Technology and Economics,  
Műgyetem rkp. 3., H-1111 Budapest, Hungary*

<sup>6</sup>*Department of Physics, University of Oradea, 410087, Oradea, Romania*

<sup>7</sup>*Institute for Advanced Study, Technical University of Munich,  
Lichtenbergstrasse 2a, 85748 Garching, Germany*

<sup>8</sup>*Department of Physics, Harvard University, Cambridge, MA 02138, USA*

<sup>9</sup>*Department of Condensed Matter Physics, Weizmann Institute of Science, Rehovot 76100, Israel.*

(Dated: July 11, 2024)

The collective tunneling of a Wigner necklace – a crystal-like state of a small number of strongly interacting electrons confined to a suspended nanotube and subject to a double well potential – is theoretically analyzed and compared with experiments in [Shapir *et al.*, *Science* **364**, 870 (2019)]. Density Matrix Renormalization Group computations, exact diagonalization, and instanton theory provide a consistent description of this very strongly interacting system, and show good agreement with experiments. Experimentally extracted and theoretically computed tunneling amplitudes exhibit a scaling collapse. Collective quantum fluctuations renormalize the tunneling, and substantially enhance it as the number of electrons increases.

## I. INTRODUCTION

While investigating correlation effects in electron liquids, Eugene Wigner conjectured in 1934 the existence of an electron crystal [1], today referred to as the *Wigner crystal*. In his seminal work, Wigner noticed that the interaction energy of a three-dimensional electron gas scales as  $E_{\text{int}} \sim n^{1/3}$  with their density  $n$ , and dominates over the kinetic energy  $E_K \sim n^{2/3}$  in the very dilute limit. Therefore, electrons must become localized at very small carrier concentrations, and form a crystal. The kinetic energy of the electrons increases upon compression, and the crystal melts due to quantum and thermal fluctuations into an electron liquid. A similar solid–liquid (quantum or thermal) phase transition occurs in two spatial dimensions [2]. In one dimension, however, quantum fluctuations destroy long-range order, and no phase transition takes place but only a crossover between a Luttinger liquid-like state and a dilute regime with power-law crystalline correlations appears [3, 4].

Since the predictions of Wigner, tremendous effort has been devoted to detect and understand this quantum crystal. While these efforts remained unsuccessful in three dimensions, Wigner crystal phases and correlations have been demonstrated in two-dimensional structures [5–29], as well as more recently in one dimension [30, 31].

Spatial confinement suppresses quantum and classical fluctuations, and stabilizes the crystalline structure. When only few electrons are confined within a limited

spatial region, one often refers to *Wigner molecules*. Such ‘molecules’ exhibit highly correlated arrangements due to the dominance of electron-electron interaction [32–36], and are characterized by significant variations in electron density as well as distinctive peaks in the density-density correlation function [37–39]. In two-dimensional quantum dots, the formation of Wigner molecules has been observed indirectly by various measurements, including transport [40, 41] and spectroscopy [42].

The real-space structure of small crystals became directly accessible recently. The structure of a small one-dimensional Wigner crystal in a carbon nanotube has been carefully probed in Ref. [30], and a *collective tunneling* of the crystal has been observed. Very recently, one-dimensional Wigner crystals have also been observed in van der Waals heterostructures [43], where the artificial stacking technique used introduces strain variations, and leads to the formation of domain walls, which exhibit unique electronic behavior, associated with the formation of a phase-locked one-dimensional Wigner crystal. By tuning the electron density, a transition can be observed from a one-dimensional Wigner crystal to a dimerized Wigner crystal, and eventually to a weakly interacting Luttinger liquid [43]. In this work, we focus on this latter phenomenon, and model and analyze the tunneling of a small, one-dimensional Wigner crystal, which we refer to as the ‘Wigner necklace’.

The setup of Ref. [30] is illustrated in Fig. 1(a). A carbon nanotube is suspended and appropriately gated.

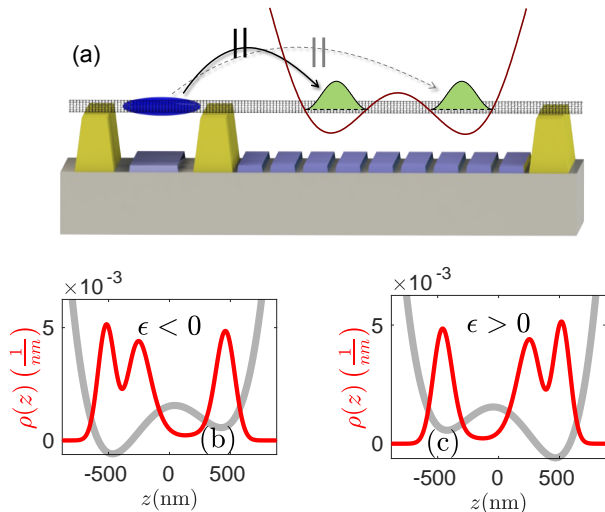


FIG. 1. (a) Experimental setup of Ref. [30] used to detect collective tunneling. The bottom gates under the nanotube are used to shape the double well potential, the left-hand-side quantum dot (dark blue) serves as a charge detector. (b) and (c) Ground state charge densities (red) from exact diagonalization for a system of three electrons in a double well potential (grey). A single electron moves between the two sides upon changing the asymmetry. The charge density displays a crystalline structure due to the strong Coulomb interaction ( $\eta = 20$  in Eq. (7)).

Gates on the right-hand side, underneath the nanotube, are utilized to trap  $N$  electrons (or holes) and create a confining potential  $V(z)$  at will, with  $z$  being the electron coordinate along the nanotube. On the left, a quantum dot is formed from the same nanotube and serves as a charge detector. The spatial structure of charge distributions within the nanotube can be further detected by placing a probe nanotube on top of the device and measuring the charge detector's response. The confining potential  $V(z)$  is well approximated by a simple quartic form,

$$V(z) = \frac{b}{4}z^4 - \frac{a}{2}z^2 - cz, \quad (1)$$

with  $a$ ,  $b$  and  $c$  tunable parameters. Tunneling between the two sides of the potential is generated by applying a bias and thereby changing the sign of  $c$ .

In the present work we investigate theoretically the collective tunneling of very strongly interacting charged particles in the potential  $V(z)$ . Such collective tunneling occurs for an odd number of particles. Then the classical ground state of the particles is twofold degenerate in a symmetrical potential, but quantum tunneling allows for the hybridization of these two states, and splits their energy. However, as demonstrated experimentally [30], due to the strong Coulomb interaction, moving just one charge from one side of the barrier to the other is accompanied by the reordering of charges and a collective motion of all

particles.

The theoretical study of this phenomenon is rather challenging in the strongly interacting regime, where usual quantum chemistry approaches break down [44]. In fact, we are not aware of any precision calculation in this regime, apart from our earlier work [30], where a special DMRG procedure has been developed to compute charge density profiles. Reaching the requested accuracy and obtaining the tunneling amplitude, however, is an even more difficult task. We apply a combination of three different methods. In the deep tunneling regime, an *instanton approach* can be used [45], but incorporating quantum fluctuations turns out to be crucial (as well as a technical challenge due to numerical instabilities) in the quantum tunneling regime. Unfortunately, most of the experimental data turn out to be in the intermediate region, where instanton theory is inapplicable. To capture the physics in this regime, too, we perform *Density Renormalization Group* (DMRG) based computations, which we corroborate with *restricted 'exact' diagonalization* calculations. These three approaches provide us a consistent picture, are in good agreement with the experimental data, and confirm the presence of collective tunneling.

Through most of this work, we neglect the electron spin. While this is not justified for intermediate interactions [39], it turns out to be an excellent approximation in the strongly interacting regime studied here. By studying the spinful  $N = 3$  case we show that in the experimentally relevant regime of large interactions *spin-charge separation* takes place, where charge degrees of freedom are responsible for the collective charge tunneling, while the spin degrees of freedom remain spectators at the experimentally relevant energies. By comparing the different theoretical methods and experiment, we also conclude that quantum fluctuations (phonons) of a small necklace enhance tunneling.

The paper is organized as follows: In Section II we outline the basic model used to describe the experimental setup of Ref. [30]. Section III is devoted to the discussion of the three complementary theoretical methods used in this work. Our results are presented in Section IV, along with a detailed comparison with the experimental data. Finally, in Section V, we study the case of  $N = 3$  spinful electrons, and demonstrate spin-charge separation. Our conclusions are summarized in Section VI, while some technical details of the instanton calculation are described in Appendix A.

## II. MODELLING THE EXPERIMENTAL SETUP

To observe the Wigner crystal regime in a carbon nanotube, the mass of the charge carriers needs to be as large as possible, and their interaction as strong as possible. The Wigner crystal regime is therefore ideally observed in suspended small diameter semiconducting nanotubes with large gaps, as the ones used in Refs. [30, 31]. Electrons confined to such nanotubes are very well described by the

effective Hamiltonian

$$H = \sum_{i=1}^N \left[ -\frac{\hbar^2}{2m^*} \frac{\partial^2}{\partial z_i^2} + V(z_i) \right] + \sum_{i<j}^N \frac{e^2}{4\pi\epsilon_0} \frac{1}{|z_i - z_j|}, \quad (2)$$

with  $m^*$  the effective mass of the electrons (holes) in the nanotube, and  $V(z)$  the confining potential, Eq. (1). The spin  $\sigma$  and the chirality  $\tau$  of the particles do not appear in this Hamiltonian [46]. They play an important role at larger electron densities [47]. However, since the tunneling experiments studied here and in Ref. [30] are performed in the spin incoherent regime [48], in most of our analysis we neglect them, and consider simply interacting spinless fermions. As we demonstrate in Section V, this is well justified in the large interaction limit, relevant for the experiments in Ref. [30], where the exchange splitting is small, spin degrees of freedom are incoherent, and the charge sector is responsible.

While they turn out to be unimportant in the very strongly interacting regime studied here, exchange interactions as well as spin-orbit interaction do play an important role at *intermediate densities*, where the Wigner crystal starts to melt; there they modify the structure of avoided level crossings in Wigner molecules [39], and lead to the emergence of magnetic correlations and magnetic phases in larger systems [31, 47].

Usually, the strength of electron-electron interaction in a homogeneous,  $d$ -dimensional electron gas is characterized by the parameter  $r_s = n^{-1/d}/a_B$ , the ratio of the typical distance between charge carriers and the Bohr radius,  $a_B = \hbar^2\epsilon/me^2$ . At  $r_s \approx 1$  the electrons' kinetic energy is approximately the same as their potential energy, while for  $r_s \gg 1$  the interaction energy dominates. It is in the latter regime that the Wigner crystal emerges.

In a confined potential, however, the concept of  $r_s$  is not particularly useful. There the confining potential sets a typical length scale, which in our case is simply the oscillator length of the quartic potential ( $a = c = 0$ ),

$$l_d = \left( \frac{\hbar^2}{m^*b} \right)^{1/6}. \quad (3)$$

Introducing the corresponding dimensionless coordinates,  $z \rightarrow \chi = z/l_d$ , defines then the natural energy scale of the problem,

$$E_0 = \frac{\hbar^2}{m^*l_d^2}, \quad (4)$$

and leads to the definition of the dimensionless strength of the Coulomb interaction [49],

$$\eta = \frac{l_d}{a_B} = \frac{m^*e^2}{\epsilon\hbar^2} \left( \frac{\hbar^2}{m^*b} \right)^{1/6}. \quad (5)$$

For the nanotube investigated here and in Ref. [30] we

obtain

$$l_d \approx 160 \text{ nm}, \quad E_0 \approx 5.56 \text{ K}, \quad \eta \approx 20, \quad (6)$$

the latter signaling an extremely strong Coulomb interaction.

In terms of these units, we obtain the dimensionless Hamiltonian

$$\tilde{H} = \sum_{i=1}^N \left[ -\frac{1}{2} \frac{\partial^2}{\partial \chi_i^2} + \frac{1}{4} \chi_i^4 - \frac{\alpha}{2} \chi_i^2 - \epsilon \chi_i \right] + \eta \sum_{i<j}^N \frac{1}{|\chi_i - \chi_j|}, \quad (7)$$

where the dimensionless parameter  $\alpha = a l_d^2/E_0$  sets the height of the tunneling barrier between the two valleys, while  $\epsilon = c l_d/E_0$  characterizes their bias.

In the following sections, we analyze this Hamiltonian by three complementary approaches: a semiclassical many-body tunneling approach, a DMRG-based quantum chemistry approach, and a restricted exact diagonalization method.

### III. THEORETICAL APPROACHES

Our goal is to compute the tunneling amplitude  $\Delta$  of the tiny crystal, i.e., the splitting of the two almost degenerate states of the necklace for  $N = \text{odd}$ , and to investigate this tunnel splitting and the electrons' charge distribution as a function of the potential height  $\alpha$ , and the bias  $\epsilon$ . The tunneling amplitude is inversely proportional to the polarizability of the Wigner molecule at  $T = 0$  temperature, and is therefore directly accessible experimentally via polarization measurements, while charge distributions can be detected by an AFM-like method using a probe nanotube [30].

#### A. Instanton theory

We first consider the Wigner necklace tunneling problem by using the instanton approach [45, 50?–52]. Instanton theory (IT) is accurate in the tunneling regime,  $\alpha \gg 0$ , however, it breaks down at small positive values,  $\alpha \lesssim \alpha_{\text{cr}}$ , with  $\alpha_{\text{cr}}$  denoting the barrier height parameter, where tunneling sets in.

In the instanton approach, one considers the imaginary time tunneling amplitude between two many-body positions. Tunneling appears as a classical motion of the particles in imaginary time, and the tunneling amplitude is proportional to  $\Delta \sim e^{-S_{\text{inst}}}$ , with  $S_{\text{inst}}$  the instanton action. Fluctuations around this classical path determine the amplitude of tunneling, i.e., the prefactor in front of the exponential [? ].

The energy splitting  $\Delta$  of the lowest lying states can be obtained by computing the imaginary time Feynman

propagator,

$$K(\chi'_0, \chi_0, \tilde{\tau}) = \langle \chi'_0 | e^{-\tau \tilde{H}} | \chi_0 \rangle, \quad (8)$$

between the minima  $\chi_0$  and  $\chi'_0$  of the many-body potential,

$$v_N(\chi) = \sum_{i=1}^N \left( -\frac{\alpha}{2} \chi_i^2 + \frac{1}{4} \chi_i^4 \right) + \eta \sum_{i<j}^N \frac{1}{|\chi_i - \chi_j|}, \quad (9)$$

with  $\tau$  the dimensionless imaginary propagation time measured in units of  $\hbar/E_0$ . One can express (8) as a path integral in terms of the imaginary time trajectories,  $\chi(\tau)$ , which are separated into a classical instanton trajectory,  $\chi_{cl}(\tau)$ , minimizing the classical (Euclidean) action

$$S_E[\chi(\tau)] = S_0 \int_0^T d\tau \left\{ \frac{1}{2} \sum_{i=1}^N \left( \frac{d\chi_i}{d\tau} \right)^2 + v_N(\chi) \right\}. \quad (10)$$

and small fluctuations around that,  $\chi(\tau) = \chi_{cl}(\tau) + \mathbf{r}(\tau)$ . The prefactor  $S_0 = (l_d/E_0)^{3/2}$  emerges naturally, and denotes the natural action unit in this problem, and  $T$  denotes the tunneling time in units of  $\hbar/E_0$ . Expanding the action to second order in  $\mathbf{r}(\tau)$  leads to the expression

$$K(\chi'_0, \chi_0, T) \approx e^{-S_{inst}} \int_{\mathbf{r}(0)=0}^{\mathbf{r}(T)=0} \mathcal{D}\mathbf{r} \exp \left\{ \frac{1}{2} \int_0^T d\tau \mathbf{r}(\tau) \cdot \left[ -\partial_\tau^2 + \partial \circ \partial v_N(\chi_{cl}(\tau)) \right] \mathbf{r}(\tau) \right\}, \quad (11)$$

with  $S_{inst} = S_E[\chi_{cl}(\tau)]$  the instanton action, and the integral accounting for quantum fluctuations around it.

We determined the initial and final equilibrium positions  $\chi_0$  and  $\chi'_0$  as well as the instanton trajectories

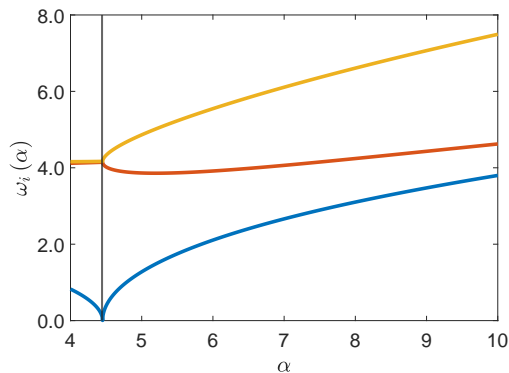


FIG. 2. Soft modes  $\omega_i$  as a function of  $\alpha$ , for  $N = 3$ . The vertical line at  $\alpha = \alpha_{cr} \approx 4.45$  marks the beginning of the tunneling regime. For  $\alpha > \alpha_{cr}$  there are two independent equilibrium positions, while for  $\alpha < \alpha_{cr}$  only one, indicating the absence of the tunneling at small  $\alpha$ .

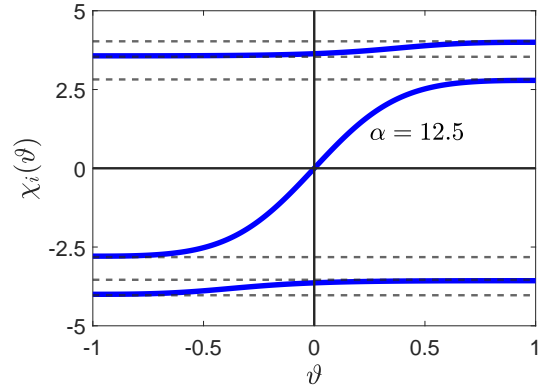


FIG. 3. Three particle imaginary time trajectories (blue) in the dimensionless units for a specific confinement parameter  $\alpha = 12.5 > \alpha_{cr}$  and  $\eta = 20$ . Dashed lines show the classical equilibrium positions or instanton turning points for the 3 particles.

by applying a Monte Carlo simulated annealing procedure [53]. Fig. 2 shows the frequencies of small vibrations around the minimum (minima) of  $v_N(\chi)$  for  $N = 3$ . The symmetrical position of the three particles becomes classically unstable at  $\alpha_{cr}^{N=3} \approx 4.45$ , the classical threshold for collective tunneling. For  $\alpha < \alpha_{cr}$  the minimum energy configuration is unique, while for  $\alpha > \alpha_{cr}$  two equilibrium positions exist, and tunneling becomes possible. The transition to the tunneling regime is marked by the softening of the lowest energy mode. Interestingly, the direction of this mode coincides with that of the instanton trajectory for  $\alpha > \alpha_{cr}$ .

A typical trajectory is displayed for  $N = 3$  particles in Fig. 3, which demonstrates collective tunneling. In our calculations, we "compactify" time by introducing the parameter  $\vartheta = \tanh(\tau/\tau_0)$ , and parametrize  $\chi$  by using  $\vartheta$ . Clearly, the middle electron tunnels through the potential barrier, while the outer electrons do not tunnel but adjust their positions.

The choice of  $\tau_0$  is important from the point of view of numerical accuracy. A small value of  $\tau_0$  increases the numerical accuracy in the tunneling region, while a large value of  $\tau_0 \approx 5$  provides better resolution around the end of the trajectories. Since the primary contribution to the energy splitting arises from the region around  $\tau \approx 0$ , a value  $\tau_0 \approx 0.5$  turns out to be optimal for accurate calculations.

Performing the Gaussian integral in Eq. (11) is a highly non-trivial task [45, 54]. The procedure consists of introducing the arc length variable  $ds^2 = d\chi_{cl}^2$  along the instanton trajectory, and  $N - 1$  perpendicular coordinates. In this way, one describes the tunneling as a one-dimensional tunneling process in an effective potential  $w(s)$ , renormalized by 'perpendicular' quantum fluctuations (see Appendix A). The tunneling amplitude is then

expressed as

$$\begin{aligned} \Delta &= R_0(\alpha, N) \Delta_1, \\ \Delta_1 &= \sqrt{\frac{4\omega_{\text{soft}}}{\pi}} \sqrt{2[v_N^{\text{max}} - v_N^{\text{min}}]} P[\chi_{\text{cl}}(s)] e^{-S_E}, \end{aligned} \quad (12)$$

with  $\Delta_1$  associated with a one-dimensional motion in the effective double-well potential, and  $R_0(\alpha, N)$  the aforementioned renormalization factor [45, 54] (see Appendix A for details). Here  $\omega_{\text{soft}}$  denotes the oscillation frequency at the initial position of the tunneling trajectory in the tunneling direction, and  $P[\chi_{\text{cl}}]$  is a renormalization factor associated with the effective one-dimensional motion. The prefactor  $R_0$  is equal to 1 for  $N = 1$ , but it becomes significant for  $N \geq 3$  (see Fig. 4), and exhibits a non-negligible  $\alpha$  dependence. Somewhat surprisingly, quantum fluctuations seem to increase the tunneling amplitude substantially, and quantitative computations must take them into account.

### B. Density matrix renormalization group

As an alternative to instanton computations, we also performed density matrix renormalization group (DMRG) computations. DMRG provides an accurate description of the intermediate tunneling regime, however, it fails in the deep tunneling regime, where we experience convergence problems.

Originally, DMRG has been proposed as an efficient computational scheme for one-dimensional systems with short-ranged interactions [55], but has been extended later to systems with long-ranged interactions as well as to higher dimensional lattices [56], and it has been reformulated more recently in a possibly more transparent way by using the language of matrix product states

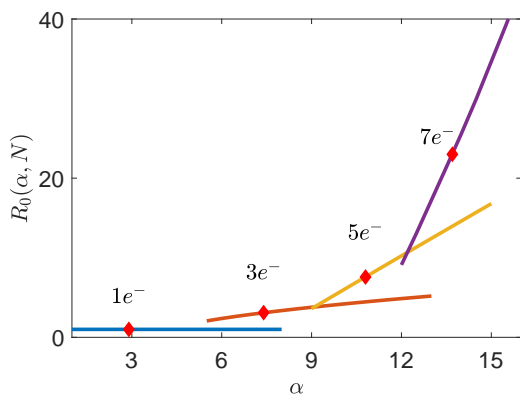


FIG. 4. Renormalization factor  $R_0(\alpha, N)$  as function of  $\alpha$  for  $N \in \{1, 3, 5, 7\}$ . On each line, the diamond symbols mark the beginning of the quantum tunneling regime.

(MPS's) [57, 58].

To perform DMRG, we express the Hamiltonian (7) in a second quantized form. The key to efficient DMRG calculations is to choose an appropriate basis in the strongly interacting limit studied here,  $\eta \gg 1$ . The most natural choice of harmonic oscillator basis functions centered at  $\chi = 0$ , e.g., is not able to reach this regime [44]. Here we perform calculations by using an *overcomplete adaptive basis* with harmonic oscillator wave functions localized around the classical equilibrium positions of the electrons [30].

In this basis, we rewrite the Hamiltonian (7) the second quantized form

$$\tilde{H} = \sum_{a,b} t_{ab} c_a^\dagger c_b + \frac{1}{2} \sum_{a,b,c,d} V_{ab,cd} c_a^\dagger c_b^\dagger c_d c_c, \quad (13)$$

where  $t_{ab}$  stands for the matrix elements of the non-interacting part of (7),  $t_{ab} = \langle \psi_a | \tilde{H}_0 | \psi_b \rangle$ , while  $V_{ab,cd} = \langle \psi_a \psi_b | U | \psi_c \psi_d \rangle$  are the matrix elements of the Coulomb interaction,  $U = \eta / |\chi - \chi'|$  calculated within the single particle wave functions described above. The computation of the matrix elements  $V_{ab,cd}$  is numerically demanding, but it can be speeded up by exploiting the translational invariance of the Coulomb interaction.

For our computations, we utilized the Budapest-DMRG code [59–61], which allows us to treat long-range interactions efficiently and to take advantage of the  $U(1)$  symmetry of the model associated with the conservation of the total charge as well as the  $Z_2$  symmetry associated with parity. In our computations, we use a bond dimension of the order of 2048-4096, and an adaptive basis consisting of 8 – 16 orbitals/electron, depending on the number of electrons. We computed the ground state energies in the even and odd parity sectors,  $E_{GS}^{(e)}$  and  $E_{GS}^{(o)}$ , and extracted the energy splitting

$$\Delta = |E_{GS}^{(e)} - E_{GS}^{(o)}|, \quad (14)$$

identified as twice the tunneling amplitude in the tunneling regime. Typical results for  $\Delta$  as well as a comparison with the results of the other approaches we used are displayed in Fig. 5 as function of  $\alpha$ . Unfortunately, in the deep tunneling regime, where  $\Delta$  becomes exponentially small,  $\Delta \lesssim 10^{-3}$ , we noticed that the convergence of DMRG was influenced by the choice of basis we utilized. Specifically, as we decreased  $\alpha$ , the states became increasingly localized, which led to convergence challenges for the desired accuracy. Although increasing the bond dimensions improves the calculations, it also demanded greater computational resources. Consequently, as an alternative approach, we employed complementary methods like restricted exact diagonalization or instanton theory to achieve accurate results. Nevertheless, the range of applicability of DMRG overlaps with that of these methods, and enables us to obtain a complete description of the collective tunneling.

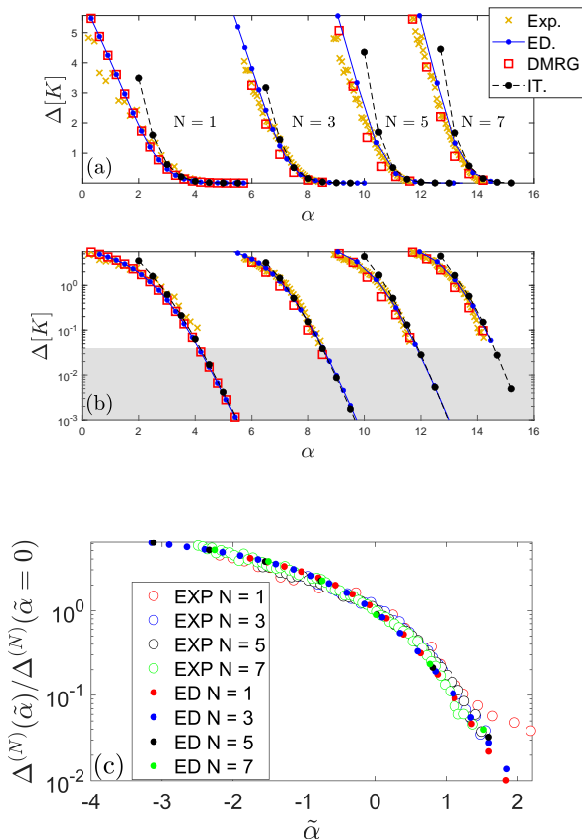


FIG. 5. (a,b) Numerically computed tunnel splitting on both linear and logarithmic scales, compared with the rescaled experimental polarization data (EXP). Instanton theory captures  $\Delta$  accurately in the deep tunneling regime, where  $\Delta$  is suppressed exponentially by increasing barrier height (see panel (b)). Each set of curves corresponds to a different number of electrons,  $N$ . The shaded region indicates the regime, where the exchange couplings may already modify the tunneling process and spin can play an important role. In panel (c), the data are scaled together and trace a single, universal curve. The tunneling regime starts at  $\tilde{\alpha} \approx 0$ .

### C. Restricted Exact Diagonalization

As a third, complementary method, we also used the restricted exact diagonalization (ED), which can be utilized to determine the eigenstates of relatively small quantum systems. Here we also use it to benchmark the other two, more sophisticated methods. In this work, we diagonalize the Hamiltonian (7) in real space.

For  $N \in \{1, 3\}$ , diagonalization is performed with a relatively large number of states,  $\sim 100$  for each particle, ensuring accurate ground state and a few excited state energies. However, for  $N \in \{5, 7\}$ , the Hilbert space becomes too large, and a complete diagonalization is impossible in practice. Nevertheless, a projected version of

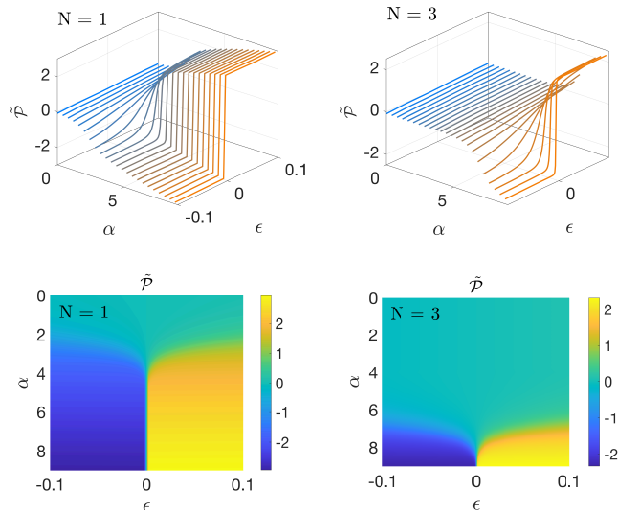


FIG. 6. Density plots for the charge polarization  $\tilde{P}(\alpha, \epsilon)$  represented as a function of  $\alpha$  and  $\epsilon$ . The polarization is calculated for  $N = 1$  and  $N = 3$  electrons inside the confinement potential.

ED can be used even in these cases, where a restricted wave function is used, with electrons treated as distinguishable particles. This method reduces the size of the Hilbert space by 2-3 orders of magnitude, and can be used to study up to  $N = 7$  electrons the low-energy spectrum in the strongly interacting limit, where exchange processes are unimportant [62].

## IV. RESULTS AND COMPARISON WITH EXPERIMENTAL DATA

### A. Polarization, polarizability, and tunneling amplitude

The careful design and control in the experiments of Ref. [30] allows one to measure the polarization  $P$  of the electrons on the nanotube as a function of the applied bias ( $\epsilon$  in Eq. (7)) as well as that of the height of the barrier, regulated by a back gate potential  $V_K$ . Such polarization results are displayed in Fig. 6 along with our theoretical calculations for  $N = 3$ .

In the theoretical computations in Fig. 6, we define the dimensionless polarization simply as

$$\tilde{P}(\alpha, \epsilon) = N \langle \chi \rangle = \int d\chi \chi \rho(\chi, \alpha, \epsilon), \quad (15)$$

with  $\rho(\chi, \alpha, \epsilon)$  the ground state charge density

$$\rho(\chi, \alpha, \epsilon) = \sum_{i=1}^N \langle \Psi | \delta(\chi - \chi_i) | \Psi \rangle, \quad (16)$$

$N$	$\alpha_0^{(N)}$	$x^{(N)}$ [meV] <sup>-1</sup>	$y^{(N)}$ [meV]	$V_0^{(N)}$ [meV]
1	2.2	14.8	1	109
3	6.9	74.2	0.25	280
5	10.4	141.9	0.15	560
7	13.2	170.8	0.13	850

TABLE I. List of rescaling parameters appearing in Eq. (18).

and  $|\Psi\rangle = |\Psi(\chi, \alpha, \epsilon)\rangle$  the ground state wave function obtained using ED or DMRG.

As one enters the quantum tunneling regime, the polarization displays a kink as a function of the applied bias. This kink becomes sharper and sharper as the barrier height increases, clearly demonstrating that the broadening of the polarization jump in the experiments is not due to thermal fluctuations, but is dominated by *quantum fluctuations* – excepting the very deep tunneling regime, where the transition becomes very sharp and its width is set by thermal fluctuations.

In this quantum tunneling regime, right at the transition,  $\epsilon = 0$ , the polarizability is inversely proportional to the tunneling amplitude,

$$\Pi = \frac{\partial P}{\partial \epsilon} \propto \frac{1}{\Delta}. \quad (17)$$

The precise prefactor here is hard to determine, since it depends on the precise charge distribution before and after the tunneling. Also, although the response at the charge sensor is certainly proportional to the polarization, it depends on the capacitive coupling between the electrons at various positions and the charge sensor. Nevertheless, the relation above enables us to extract the tunneling amplitude as a function of the shape of the barrier, apart from an overall scale.

For a detailed comparison with the experiments, we assumed that there is a linear relation between the voltage  $V_K$  and the dimensionless parameter  $\alpha$ . This leads to the relations

$$\begin{aligned} \alpha^{(N)} &= \alpha_0^{(N)} + x^{(N)} (V_K - V_0^{(N)}), \\ \Delta^{(N)} &= y^{(N)} \frac{\Pi^{(N)}(V_0^{(N)})}{\Pi^{(N)}(V_K)}. \end{aligned} \quad (18)$$

Here the parameters  $\alpha_0^{(N)}$  and  $V_0^{(N)}$  mark the threshold of tunneling regime, while  $x^{(N)}$  and  $y^{(N)}$  rescale the axes. We obtain a remarkably accurate fit to the experiments, as displayed in Fig. 5. Our fitting parameters are enumerated in Table I; both  $\alpha_0^{(N)}$  and  $x^{(N)}$  scale roughly linearly with the threshold,  $V_0^{(N)}$ , while the overall polarizability rescaling coefficient scales as  $y^{(N)} \sim 1/N$ . Interestingly, the data obtained for various  $N$  values also display a universal scaling when plotted as a function of  $\tilde{\alpha} = \alpha - \alpha_0$ , as demonstrated in Fig. 5.

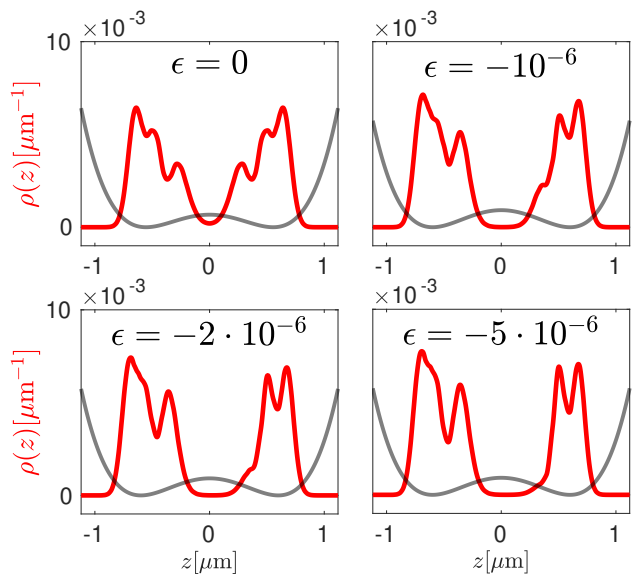


FIG. 7. Charge distribution profiles for  $N = 5$  particles, with different  $\epsilon$  values. At  $\epsilon = 0$  the particle in the middle is represented on both sides of the potential barrier, while by increasing the linear detuning, we see that it slowly shifts to one side, changing the positions for the side particles as well.

## B. Charge distribution and polarization

The experimental set-up of Ref. [30] also allows measuring charge distributions. In particular, the collective motion of the electrons has been demonstrated by measuring the difference of the charge density,  $\Delta\rho(z, \alpha, \epsilon)$ , before and after the tunneling, and comparing the results with theoretical computations for  $N = 3$  (see Fig. 4 in Ref. [30]).

Although experimentally it is not possible to measure non-invasively  $\rho(z)$  at the most interesting point,  $\epsilon = 0$ , we can compute  $\rho(z)$  for any value of  $\epsilon$ , and study its evolution upon changing the bias. The redistribution of charge as a function of bias, as obtained via ED computations is displayed in Fig. 7 for  $N = 5$  particles. While for  $\epsilon \gg \Delta$  two electrons reside on the right and three on the left, for  $\epsilon \approx 0$  the system delocalizes between the "2+3" and "3+2" states, as reflected by the deformation of the density profile. While the motion of the central electron is certainly dominant, the profile difference,  $\Delta\rho(z)$ , presented in Fig. 8, clearly indicates that all charges are displaced in course of the quantum tunneling process.

We present  $\rho(\chi)$  for  $N = 3$  particles in Fig. 10 for a set of parameters  $\alpha$ . The classical ground state becomes twofold degenerate at  $\alpha = \alpha_{cl}^{N=3} \approx 4.45$ . Quantum fluctuations, however, shift this threshold to  $\alpha_0^{N=3} \approx 6.9$ , and tunneling takes place only for  $\alpha \gtrsim 6.3$ . Fig. 10 also displays the charge polarization, Eq. (15). The main contribution to the polarization comes from the tunneling of the central electron, and the rearrangement of electrons on the right and the left yields a much smaller contribution.

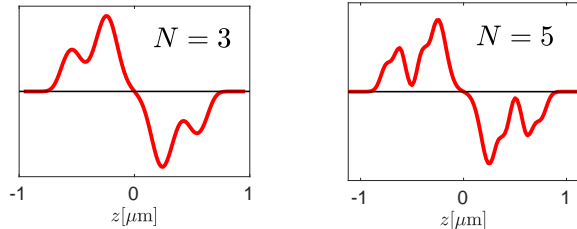


FIG. 8. Smeared charge density difference,  $\Delta\rho(z)$ , between the left and right polarized states for  $N = 3$  and  $N = 5$  as a function of the bias,  $\epsilon$ . The peaks emerging on the sides indicates, that during the tunneling all the three particles change their positions.

At  $\epsilon \approx 0$ , the central electron is strongly delocalized between the two sides, while the lateral electrons gradually shift as the central charge is transferred.

This seems to suggest that lateral electrons are merely spectators of the tunneling event. This is, however, not true. As already discussed above, the profile  $\Delta\rho$  clearly demonstrates that *all electrons* participate in the tunneling process. This is corroborated by our instanton computations, which show that lateral electrons participate in collective vibrations and thereby enhance quantum fluctuations, which largely facilitate the quantum-tunneling process, as captured by the increased prefactor  $R_0$  in Eq. (12).

## V. THE ROLE OF SPIN AND VALLEY DEGREES OF FREEDOM

In this section, we investigate the role of the spin degrees of freedom, and demonstrate that they do not play a significant role in the experimentally accessible regime for large interactions,  $\eta \approx 20$ . In addition to spin, electrons in nanotubes also possess a chirality (spin) [63]. These play a role similar to ordinary spins in nanotubes. In the small diameter nanotubes used in [30], however, spin-orbit coupling is strong [63]. Therefore, at the energy scales investigated here, chiral quantum numbers are already merged with spin degrees of freedom in to a composite  $SU(2)$  degree of freedom, replacing the electrons' ordinary spin [47]. Spin in the following refers to this composite degree of freedom.

Studying this large interaction range,  $\eta \sim 20$  is extremely demanding, and we are not aware of any reliable computation in this regime. In this regime, a much larger and adaptive basis [30] is needed to capture the physics at all relevant length scales and reach the accuracy requested to determine the size of (exponentially small) level crossings. Here we therefore focus only on the case of  $N = 3$  and include only the electrons' composite spin, i.e., we focus on small diameter nanotubes and energy scales below a few Kelvins.

The evolution of the ground state energy and that of a few excited states is computed by varying the potential height  $\alpha$ . The spinful DMRG approach [60] is employed as the method of analysis, utilizing an over-complete harmonic oscillator basis, centered at around the classical equilibrium positions before and after tunneling [30]. The calculation employs a total of 24 spinfull orbitals, and a DMRG bond dimension  $M = 2048$ , guaranteeing an accuracy of around  $\sim 10^{-5}$  in terms of the Schmidt values, corresponding to an energy precision of around  $\sim 10^{-2}$  K.

Fig. 9 demonstrates the energy spectrum's dependence on  $\alpha$  for intermediate ( $\eta = 4$ , panel (a)), and strong ( $\eta = 20$ , panel (b)) interactions. For intermediate interactions (panel (a)), the spin degrees of freedom play a significant role: the ground state is a doublet in agreement with prior results [39]. The excitation spectrum observed can be interpreted very differently for small and large values of  $\alpha$ .

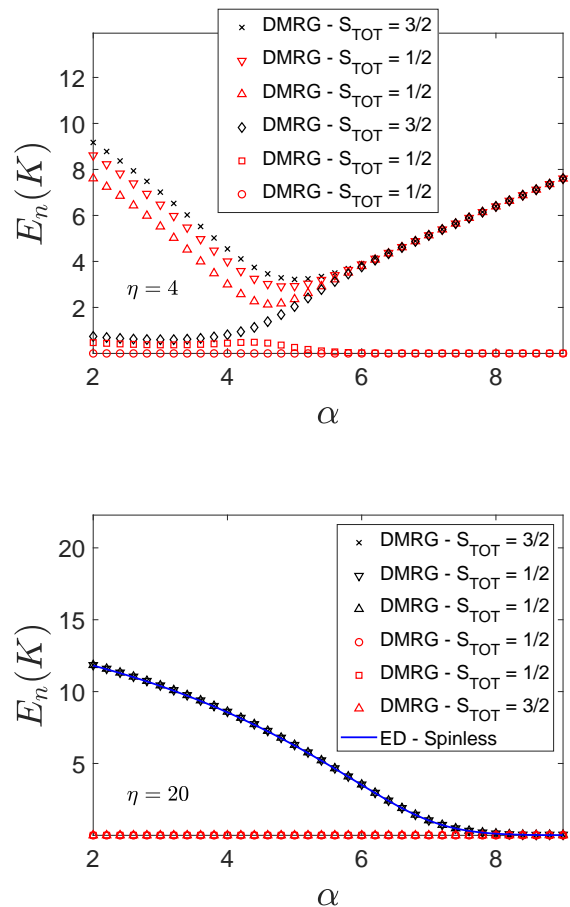


FIG. 9. The energy spectrum of three electrons with spin confined in a double well potential is depicted, illustrating the influence of spin degrees of freedom under both (a) weak Coulomb interactions with  $\eta = 4$  and (b) the strong coupling limit with  $\eta = 20$ , as a function of the parameter  $\alpha$ .



In the limit of small  $\alpha \lesssim 5$ , the excitation spectrum can be understood as a spectrum of a small,  $N = 3$  Wigner necklace: in this case the electrons form a small spin chain with a doublet ground state, and their spin excitations are well described by the effective Hamiltonian,

$$H_{\text{eff}} = J(\mathbf{S}_1 + \mathbf{S}_3)\mathbf{S}_2,$$

The ground state and the first excited states of this Hamiltonian are doublets, separated by the exchange energy  $E_1 - E_0 = J$ , while the highest excited state is a spin  $S = 3/2$  multiplet, located at an energy  $E_2 - E_0 = 3J/2$ , in good agreement with the spectrum presented in Fig. 9, and an exchange interaction,  $J \approx 0.5$  K. The excited states at around 8K exhibit a strikingly similar spin structure. They can be interpreted as a collective vibrational charge excitation, decorated by the spin excitations of the Wigner necklace, with a slightly increased value of the exchange coupling,  $J$ .

The interpretation of the  $\alpha \gtrsim 5$  spectrum for  $\eta = 4$  is, however, rather different. At large  $\alpha$ , two electrons are forced to reside on one side of the barrier, and the strength of the potential that squeezes them together increases linearly with  $\alpha$ . As a result, for  $\eta = 4$  and  $\alpha \gtrsim 5$ , these two electrons do *not* form a Wigner molecule, but rather, they occupy the ground state of the confining potential, forming a singlet. These two electrons can tunnel between the r.h.s. and the l.h.s. of the barrier, yielding an even spin  $S = 1/2$  ground state and an almost degenerate odd state of spin  $1/2$ . The splitting between these states can be identified as the quantum tunneling amplitude.

The other, higher energy excited states for  $\alpha \gtrsim 5$  and  $\eta = 4$  can be explained similarly, but in this case one of the electrons resides on the excited state, and forms a triplet by Hund's rule. This triplet can form a spin  $S = 1/2$  and a spin  $S = 3/2$  state with the electron on the other side of the barrier, and form even and odd states, yielding a group of four excited multiplets, two of  $S = 3/2$ , and two other of  $S = 1/2$ .

In the strong coupling limit,  $\eta = 20$ , the spectrum changes substantially (see Fig. 9(b)). In this regime, the exchange couplings are suppressed, and electrons form a Wigner molecule, even when confined to one side. As a result, charge degrees of freedom play the dominant role, and the levels form almost spin degenerate 'bundles'.

For  $\alpha \lesssim 6$ , ground state and the seven almost degenerate low-energy excitations correspond to the spin states of an  $N = 3$  Wigner necklace, consisting of two almost degenerate doublets and a triplet. The first excitation 'bundle' can be interpreted as the first collective charge excitation of the molecule, with the spins remaining spectators only.

Upon increasing the barrier  $\alpha$ , the first excitation, identified for small  $\alpha$  as a collective vibrational charge mode, becomes softer and softer, and gradually turns into a tunneling mode between the charge states  $(N_L, N_R) = (2, 1)$  and  $(1, 2)$ . Notice that for  $\eta \approx 20$ , the spins play the role of silent degeneracy labels even for  $\alpha \gtrsim 6$ .

For comparison, we have also displayed in panel (b)

the energy levels obtained by solving the Schrödinger equation for three spinless, interacting particles in real space (solid blue line), demonstrating that the electrons' spin is almost redundant, and the amplitude of tunneling is determined simply by charge excitations.

These findings confirm that, in the strongly interacting regime,  $\eta \approx 20$ , it is safe to neglect spin degrees of freedom and consider electrons as spinless particles as long as the tunnel splitting associated with the charge degrees of freedom remains larger than the exchange splitting, which for  $\eta = 20$  and  $N = 3$  is approximately  $\Delta_{\text{min}} \approx 0.03$  K. This threshold is just below the smallest experimentally observed tunneling amplitude.

## VI. CONCLUSION

In this work, we combined several theoretical approaches to describe the tunneling of a tiny Wigner crystal confined within a suspended carbon nanotube and subject to a double-well potential, studied experimentally in Ref. [30]. For an odd number of electrons and for sufficiently high barriers, the classical ground state of the Wigner molecule becomes degenerate, and the necklace tunnels between these two states.

A combination of instanton theory, Density Matrix Renormalization Group and a peculiar Exact Diagonalization method allowed us to describe the low energy spectrum of the necklace as well as its charge distribution, and determine the amplitude of collective tunneling in this very strongly interacting regime, and compare with the experimental results [30]. The methods above provide us a consistent picture, compare well with the experiments, and provide a quantitative theory for the experimental data in Ref. [30].

Interestingly, the tunneling crossover does not take place at the classical bifurcation point, as naively expected, but due to quantum fluctuations it is shifted towards somewhat higher barrier values (higher values of  $\alpha$  in Eq. (7)). Indeed, our calculations clearly demonstrate both the importance of quantum fluctuations and the collective nature of tunneling.

Rather surprisingly, we find that the presence of other particles *increases* the tunneling amplitude rather than reducing it. Indeed, in typical tunneling problems the presence of environment leads to a *suppression* of tunneling due to Anderson's orthogonality catastrophe [64, 65]. The physics behind this latter phenomenon is that the motion of one (test) particle influences the wave function of all other particles, too, which therefore act back and suppress the motion of aforementioned particle. In our case, however, collective quantum fluctuations of the electron chain seem to play a much more important role: they facilitate the motion of the innermost electron, which is mostly responsible for the tunneling. This effect is very similar to the one found in the case of infinitely long one-dimensional chains, where quantum fluctuations can strongly *suppress* the strength of a pinning center, even

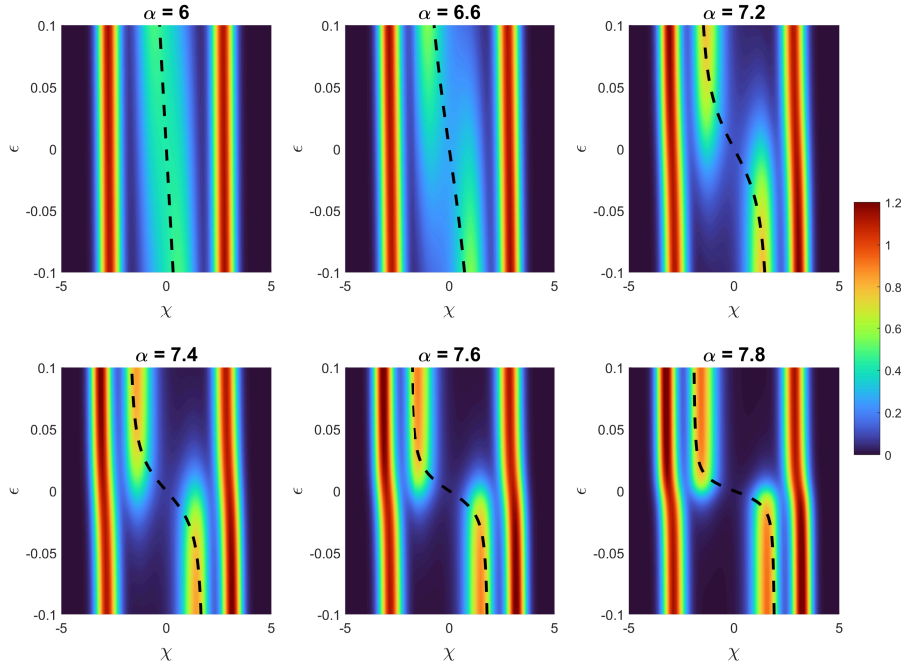


FIG. 10. Charge distribution (color code) and the polarization (dashed line) for  $N = 3$  particles. The classical critical point is at  $\alpha_{\text{cl}}^{N=3} \approx 4.45$ , but tunneling occurs only above  $\alpha_0^{N=3} \approx 6.9$ . Most of the polarization is carried by the central electron. Quantum fluctuations of lateral electrons facilitate the tunneling process.

in the limit of very strong interactions,  $r_s \gg 1$ , where pinning is a strongly relevant perturbation [66, 67].

Quite astonishingly, the experimental data as well as our theoretical curves exhibit a universal scaling collapse. At a first sight, this seems quite natural: one can identify a single collective coordinate within the instanton theory, which moves in an effective double well potential, and is responsible for the tunneling of the tiny crystal. This would support the emergence of a universal tunneling curve – apart from some overall scaling factors. However, the remaining degrees of freedom renormalize the tunneling amplitude for  $N \geq 3$  particles by a renormalization factor that has an intrinsic gate voltage dependence. Apparently, the latter renormalization factor, although without an obvious reason, does not spoil the aforementioned universal scaling within our computational accuracy.

Finally, let us discuss the role of spin and chiral degrees of freedom in the strongly interacting regime, studied here. Electrons or holes in a nanotube possess chirality and spin quantum numbers. For the nanotubes used in the experiments in Ref. [30], the large SO coupling freezes spins and chiral spins into a single composite spin below a few Kelvins [47]. We performed DMRG calculations for  $N = 3$  particles, where we incorporate the effect of this composite spin. We find that this composite  $SU(2)$  spin plays an important role for moderate interactions,  $\eta \sim 5$ , in agreement with the results of Ref. [39], and there

it modifies the structure of avoided level crossings, i.e., the tunneling process. In the strongly interacting regime studied experimentally in Ref. [30],  $\eta \approx 20$ , however, we find that spins behave as ‘spectators’, and the tunneling process is well-described simply in terms of charge degrees of freedom and spinless particles. Neglecting the spin degrees of freedom is therefore well-justified when analyzing the experiments in Ref. [30].

In two-dimensional experiments, a strong magnetic field is often applied to shrink the cyclotron orbitals, and aid the formation of a Wigner crystal [8, 11, 68, 69]. In contrast, a one-dimensional systems such as carbon nanotubes, the magnetic field does not compress the orbitals. Rather, it couples to the chirality and the spin of the electrons or holes via the Zeeman coupling, and splits spin and chirality degeneracies [47]. Transport experiments through the Wigner crystal in the co-tunneling regime in a magnetic field could unveil the spin and chirality structure of the ground and excited states.

At very low temperatures or smaller interactions, however, exchange processes may become important, and disregarding the spin sector entirely is not quite appropriate [48, 70]. This may be further complicated by the presence of spin-orbit coupling, especially in larger diameter nanotubes: spin-orbit interaction couples spin and chiral degrees of freedom, and leads to the freezing of the charge carriers’  $SU(4)$  spin. The description of the

residual SU(2) degrees of freedom [47] and their impact on the tunneling process at low temperatures as well as the role of the SU(4)→SU(2) cross-over is an open and very challenging problem, which requires further investigation.

### ACKNOWLEDGMENTS

This research is supported by the National Research, Development and Innovation Office NKFIH through research grants Nos. K134983, and K132146, and within the Quantum Information National Laboratory of Hungary (Grant No. 2022-2.1.1-NL-2022-00004). M.A.W. has also been supported by the Janos Bolyai Research Scholarship of the Hungarian Academy of Sciences and by the ÚNKP-22-5-BME-330 New National Excellence Program of the Ministry for Culture and Innovation from the source of the National Research, Development and Innovation Fund C.P.M acknowledges support by the Ministry of Research, Innovation and Digitization, CNCS/CCCDI-UEFISCDI, under projects number PN-III-P4-ID-PCE-2020-0277 and the project for funding the excellence, contract No. 29 PFE/30.12.2021. O.L. has been supported by Scalable and Predictive methods for Excitation and Correlated phenomena (SPEC), funded as part of the Computational Chemical Sciences Program by the U.S. Department of Energy (DOE), Office of Science, Office of Basic Energy Sciences, Division of Chemical Sciences, Geosciences, and Biosciences at Pacific Northwest National Laboratory. D.S. acknowledges the professional support of the doctoral student scholarship program of the co-operative doctoral program of the Ministry for Innovation and Technology from the source of the National Research, Development and Innovation fund.

### Appendix A: Computation of the instanton prefactor.

Performing the Gaussian integral in Eq. (11), one finds [45]

$$K(\chi'_0, \chi_0) = e^{-S_E} \sqrt{\frac{2S_E}{\pi}} \left[ \frac{\det'(-\partial_\vartheta^2 + V_0''(\vartheta))}{\det(-\partial_\vartheta^2 + \omega_{\text{soft}}^2)} \right]^{-1/2} \times \left[ \frac{\det'(-\partial_\vartheta^2 \mathbf{1} + \mathbf{\Omega}^2(\vartheta))}{\det(-\partial_\vartheta^2 \mathbf{1} + \mathbf{\Omega}_0^2)} \right]^{-1/2}. \quad (\text{A1})$$

Here the first line represents the propagator's classical contribution, whereas the second line denotes the contribution arising from quantum fluctuations.

The softest vibrational mode at the base of the classical trajectory  $\chi_{cl}(\tau)$  has a frequency  $\omega_{\text{soft}}$ , and  $\det'$  denotes the functional determinant, computed by excluding the

zero eigenvalue in the energy spectrum of the tunneling.

The  $(N-1) \times (N-1)$  matrix  $\mathbf{\Omega}_0$  represents the eigenfrequencies around the equilibrium position,  $\chi_0$ . The  $(N-1) \times (N-1)$  matrix  $\mathbf{\Omega}(\vartheta)$  is computed using the vibrational eigenvectors along the instanton trajectory. Technically, to compute the contribution coming from the quantum fluctuations is a delicate issue. We followed the approach introduced in Ref. [45] and introduce the Jacobian fields through  $(-\partial_\vartheta^2 \mathbf{1} + \mathbf{\Omega}^2(\vartheta)) \mathbf{J}(\vartheta) = 0$  which is related with the derivative of the instanton  $\kappa(\vartheta) \propto \dot{\chi}(\vartheta)$ . Introducing a function  $\mathbf{\Xi}(\vartheta) = \dot{\kappa}(\vartheta) \kappa(\vartheta)^{-1}$  that satisfies a differential equation,  $\dot{\mathbf{\Xi}} = \varrho/(1-\vartheta^2) (\mathbf{\Omega}^2(\vartheta) - \mathbf{\Xi}^2(\vartheta))$ , with the boundary condition that the particles behavior is of a harmonic oscillator, we can express the tunnel splitting in a compact form.

An essential aspect of this calculation is the introduction of a coordinate basis transformation on the  $N$  dimensional trajectory. The new basis consists of one parallel and  $N-1$  perpendicular unit vectors with respect to the trajectory, as opposed to  $N$  coordinates that describe the independent particles. It is found that the trajectory's direction is parallel to the eigenvector of the softest vibrational eigenmode.

In this description the trajectory and subsequent calculations can be simplified to an arc-length parametrized effectively one-dimensional description. This takes place in the effective potential, that is created by the collective motion of particles as in Fig. 3. This enables us to calculate the quantity  $P[\chi_{cl}(s)]$  as a one-dimensional equation. This renormalization constant depends on the momentum-like quantity  $p_0 = \sqrt{2[v_N^{\text{max}} - v_N^{\text{min}}]}$

$$P[\chi_{cl}(s)] = \exp \left\{ \int_{-1}^0 d\vartheta \frac{\varrho}{(1-\vartheta^2)} \left( \omega_{\text{soft}} - \frac{\partial p_0(s)}{\partial s} \right) \right\}. \quad (\text{A2})$$

This arc-length parametrized picture makes it possible to express  $\mathbf{\Omega}$  by the curvature of the trajectory parametrized either by imaginary time or arc-length, although the two descriptions yield the same results. Solving numerically the set of differential equations  $\dot{\mathbf{\Xi}} = \varrho/(1-\vartheta^2) (\mathbf{\Omega}^2(\vartheta) - \mathbf{\Xi}^2(\vartheta))$  with the appropriate boundary conditions that states, that indeed for times close to  $\vartheta = \pm 1$  the particles behave like a collective harmonic oscillator.

The renormalization factor  $R_0(\alpha, N)$  then can be expressed as

$$R_0(\alpha, N) = \sqrt{\frac{\det \mathbf{\Omega}_0}{\det \mathbf{\Xi}(0)}} \times \exp \left\{ \int_{-1}^0 d\vartheta \frac{\varrho}{(1-\vartheta^2)} \text{Tr}(\mathbf{\Omega}_0 - \mathbf{\Xi}(\vartheta)) \right\}. \quad (\text{A3})$$

- [1] E. Wigner, On the interaction of electrons in metals, *Phys. Rev.* **46**, 1002 (1934).
- [2] L. Bonsall and A. A. Maradudin, Some static and dynamical properties of a two-dimensional wigner crystal, *Phys. Rev. B* **15**, 1959 (1977).
- [3] H. J. Schulz, Wigner crystal in one dimension, *Phys. Rev. Lett.* **71**, 1864 (1993).
- [4] J. S. Meyer and K. A. Matveev, Wigner crystal physics in quantum wires, *Journal of Physics: Condensed Matter* **21**, 023203 (2008).
- [5] C. C. Grimes and G. Adams, Evidence for a liquid-to-crystal phase transition in a classical, two-dimensional sheet of electrons, *Phys. Rev. Lett.* **42**, 795 (1979).
- [6] D. S. Fisher, B. I. Halperin, and P. M. Platzman, Phonon-ripplon coupling and the two-dimensional electron solid on a liquid-helium surface, *Phys. Rev. Lett.* **42**, 798 (1979).
- [7] F. Gallet, G. Deville, A. Valdès, and F. I. B. Williams, Fluctuations and shear modulus of a classical two-dimensional electron solid: Experiment, *Phys. Rev. Lett.* **49**, 212 (1982).
- [8] D. C. Tsui, H. L. Stormer, and A. C. Gossard, Two-dimensional magnetotransport in the extreme quantum limit, *Phys. Rev. Lett.* **48**, 1559 (1982).
- [9] E. Y. Andrei, G. Deville, D. C. Glattli, F. I. B. Williams, E. Paris, and B. Etienne, Observation of a magnetically induced wigner solid, *Phys. Rev. Lett.* **60**, 2765 (1988).
- [10] H. W. Jiang, R. L. Willett, H. L. Stormer, D. C. Tsui, L. N. Pfeiffer, and K. W. West, Quantum liquid versus electron solid around  $\nu=1/5$  landau-level filling, *Phys. Rev. Lett.* **65**, 633 (1990).
- [11] V. J. Goldman, M. Santos, M. Shayegan, and J. E. Cunningham, Evidence for two-dimensional quantum wigner crystal, *Phys. Rev. Lett.* **65**, 2189 (1990).
- [12] H. Buhmann, W. Joss, K. von Klitzing, I. V. Kukushkin, A. S. Plaut, G. Martinez, K. Ploog, and V. B. Timofeev, Novel magneto-optical behavior in the wigner-solid regime, *Phys. Rev. Lett.* **66**, 926 (1991).
- [13] M. B. Santos, J. Jo, Y. W. Suen, L. W. Engel, and M. Shayegan, Effect of landau-level mixing on quantum-liquid and solid states of two-dimensional hole systems, *Phys. Rev. B* **46**, 13639 (1992).
- [14] K. Shirahama and K. Kono, Dynamical transition in the wigner solid on a liquid helium surface, *Phys. Rev. Lett.* **74**, 781 (1995).
- [15] J. Yoon, C. C. Li, D. Shahar, D. C. Tsui, and M. Shayegan, Wigner crystallization and metal-insulator transition of two-dimensional holes in gaas at  $B = 0$ , *Phys. Rev. Lett.* **82**, 1744 (1999).
- [16] Y. P. Chen, G. Sambandamurthy, Z. H. Wang, R. M. Lewis, L. W. Engel, D. C. Tsui, P. D. Ye, L. N. Pfeiffer, and K. W. West, Melting of a 2d quantum electron solid in high magnetic field, *Nature Physics* **2**, 452 (2006).
- [17] F. Cavaliere, U. D. Giovannini, M. Sasseti, and B. Kramer, Transport properties of quantum dots in the wigner molecule regime, *New Journal of Physics* **11**, 123004 (2009).
- [18] H. Zhu, Y. P. Chen, P. Jiang, L. W. Engel, D. C. Tsui, L. N. Pfeiffer, and K. W. West, Observation of a pinning mode in a wigner solid with  $\nu = 1/3$  fractional quantum hall excitations, *Phys. Rev. Lett.* **105**, 126803 (2010).
- [19] L. Tiemann, T. D. Rhone, N. Shibata, and K. Muraki, Nmr profiling of quantum electron solids in high magnetic fields, *Nature Physics* **10**, 648 (2014).
- [20] H. Deng, Y. Liu, I. Jo, L. N. Pfeiffer, K. W. West, K. W. Baldwin, and M. Shayegan, Commensurability oscillations of composite fermions induced by the periodic potential of a wigner crystal, *Phys. Rev. Lett.* **117**, 096601 (2016).
- [21] H. Deng, L. N. Pfeiffer, K. W. West, K. W. Baldwin, L. W. Engel, and M. Shayegan, Probing the melting of a two-dimensional quantum wigner crystal via its screening efficiency, *Phys. Rev. Lett.* **122**, 116601 (2019).
- [22] M. K. Ma, K. A. Villegas Rosales, H. Deng, Y. J. Chung, L. N. Pfeiffer, K. W. West, K. W. Baldwin, R. Winkler, and M. Shayegan, Thermal and quantum melting phase diagrams for a magnetic-field-induced wigner solid, *Phys. Rev. Lett.* **125**, 036601 (2020).
- [23] E. C. Regan, D. Wang, C. Jin, M. I. Bakti Utama, B. Gao, X. Wei, S. Zhao, W. Zhao, Z. Zhang, K. Yumigeta, M. Blei, J. D. Carlström, K. Watanabe, T. Taniguchi, S. Tongay, M. Crommie, A. Zettl, and F. Wang, Mott and generalized wigner crystal states in wse2/ws2 moirésuperlattices, *Nature* **579**, 359 (2020).
- [24] T. Smoleński, P. E. Dolgirev, C. Kuhlenkamp, A. Popert, Y. Shimazaki, P. Back, X. Lu, M. Kroner, K. Watanabe, T. Taniguchi, I. Esterlis, E. Demler, and A. Imamoğlu, Signatures of wigner crystal of electrons in a monolayer semiconductor, *Nature* **595**, 53 (2021).
- [25] Y. Zhou, J. Sung, E. Brutschea, I. Esterlis, Y. Wang, G. Scuri, R. J. Gelly, H. Heo, T. Taniguchi, K. Watanabe, G. Zaránd, M. D. Lukin, P. Kim, E. Demler, and H. Park, Bilayer wigner crystals in a transition metal dichalcogenide heterostructure, *Nature* **595**, 48 (2021).
- [26] H. Li, S. Li, E. C. Regan, D. Wang, W. Zhao, S. Kahn, K. Yumigeta, M. Blei, T. Taniguchi, K. Watanabe, S. Tongay, A. Zettl, M. F. Crommie, and F. Wang, Imaging two-dimensional generalized wigner crystals, *Nature* **597**, 650 (2021).
- [27] K. A. Villegas Rosales, S. K. Singh, M. K. Ma, M. S. Hossain, Y. J. Chung, L. N. Pfeiffer, K. W. West, K. W. Baldwin, and M. Shayegan, Competition between fractional quantum hall liquid and wigner solid at small fillings: Role of layer thickness and landau level mixing, *Phys. Rev. Res.* **3**, 013181 (2021).
- [28] J. Falson, I. Sodemann, B. Skinner, D. Tabrea, Y. Kozuka, A. Tsukazaki, M. Kawasaki, K. von Klitzing, and J. H. Smet, Competing correlated states around the zero-field wigner crystallization transition of electrons in two dimensions, *Nature Materials* **21**, 311 (2022).
- [29] M. S. Hossain, M. K. Ma, K. A. Villegas-Rosales, Y. J. Chung, L. N. Pfeiffer, K. W. West, K. W. Baldwin, and M. Shayegan, Anisotropic two-dimensional disordered wigner solid, *Phys. Rev. Lett.* **129**, 036601 (2022).
- [30] I. Shapir, A. Hamo, S. Pecker, C. P. Moca, Ö. Legeza, G. Zarand, and S. Ilani, Imaging the electronic wigner crystal in one dimension, *Science* **364**, 870 (2019).
- [31] V. V. Deshpande and M. Bockrath, The one-dimensional wigner crystal in carbon nanotubes, *Nature Physics* **4**, 314 (2008).
- [32] L. Wendler, V. M. Fomin, A. V. Chaplik, and A. O. Govorov, Optical properties of two interacting electrons in quantum rings: Optical absorption and inelastic light scattering, *Phys. Rev. B* **54**, 4794 (1996).

- [33] R. Egger, W. Häusler, C. H. Mak, and H. Grabert, Crossover from fermi liquid to wigner molecule behavior in quantum dots, *Phys. Rev. Lett.* **82**, 3320 (1999).
- [34] C. Ellenberger, T. Ihn, C. Yannouleas, U. Landman, K. Ensslin, D. Driscoll, and A. C. Gossard, Excitation spectrum of two correlated electrons in a lateral quantum dot with negligible zeeman splitting, *Phys. Rev. Lett.* **96**, 126806 (2006).
- [35] C. Yannouleas and U. Landman, Symmetry breaking and quantum correlations in finite systems: studies of quantum dots and ultracold bose gases and related nuclear and chemical methods, *Reports on Progress in Physics* **70**, 2067 (2007).
- [36] J. Corrigan, J. P. Dodson, H. E. Ercan, J. C. Abadillo-Uriel, B. Thorgrimsson, T. J. Knapp, N. Holman, T. McJunkin, S. F. Neyens, E. R. MacQuarrie, R. H. Foote, L. F. Edge, M. Friesen, S. N. Coppersmith, and M. A. Eriksson, Coherent control and spectroscopy of a semiconductor quantum dot wigner molecule, *Phys. Rev. Lett.* **127**, 127701 (2021).
- [37] P. A. Maksym, H. Imamura, G. P. Mallon, and H. Aoki, Molecular aspects of electron correlation in quantum dots, *Journal of Physics: Condensed Matter* **12**, R299 (2000).
- [38] K. Jauregui, W. Häusler, and B. Kramer, Wigner molecules in nanostructures, *Europhysics Letters* **24**, 581 (1993).
- [39] C. Yannouleas and U. Landman, Molecular formations and spectra due to electron correlations in three-electron hybrid double-well qubits, *Phys. Rev. B* **105**, 205302 (2022).
- [40] S. Tarucha, D. G. Austing, T. Honda, R. J. van der Hage, and L. P. Kouwenhoven, Shell filling and spin effects in a few electron quantum dot, *Phys. Rev. Lett.* **77**, 3613 (1996).
- [41] L. H. Kristinsdóttir, J. C. Cremon, H. A. Nilsson, H. Q. Xu, L. Samuelson, H. Linke, A. Wacker, and S. M. Reimann (Nanometer Structure Consortium, nmC@LU), Signatures of wigner localization in epitaxially grown nanowires, *Phys. Rev. B* **83**, 041101 (2011).
- [42] A. M. Mintairov, D. V. Lebedev, N. Bert, K. G. Belyaev, V. N. Nevedomskiy, M. V. Rakhlin, A. A. Toropov, A. S. Vlasov, A. Gocalinska, G. Juska, E. Pelucchi, M. A. Arredondo, A. B. Naden, A. V. Shelaev, and V. A. Bykov, Atomic ordering and bond relaxation in optical spectra of self-organized InP/GaInP<sub>2</sub> Wigner molecule structures, *Applied Physics Letters* **115**, 202104 (2019), [https://pubs.aip.org/aip/apl/article-pdf/doi/10.1063/1.5126527/14527701/202104\\_1\\_online.pdf](https://pubs.aip.org/aip/apl/article-pdf/doi/10.1063/1.5126527/14527701/202104_1_online.pdf).
- [43] H. Li, Z. Xiang, T. Wang, M. H. Naik, W. Kim, J. Nie, S. Li, Z. Ge, Z. He, Y. Ou, R. Banerjee, T. Taniguchi, K. Watanabe, S. Tongay, A. Zettl, S. G. Louie, M. P. Zaletel, M. F. Crommie, and F. Wang, Imaging tunable luttinger liquid systems in van der waals heterostructures, *ArXiv* **10.48550/ARXIV.2404.16344** (2024).
- [44] A. Secchi and M. Rontani, Wigner molecules in carbon-nanotube quantum dots, *Phys. Rev. B* **82**, 035417 (2010).
- [45] G. V. Mil'nikov and H. Nakamura, Practical implementation of the instanton theory for the ground-state tunneling splitting, *The Journal of Chemical Physics* **115**, 6881 (2001).
- [46] J.-C. Charlier, X. Blase, and S. Roche, Electronic and transport properties of nanotubes, *Rev. Mod. Phys.* **79**, 677 (2007).
- [47] L. Sárkány, E. Szirmai, C. P. Moca, L. Glazman, and G. Zaránd, Wigner crystal phases in confined carbon nanotubes, *Phys. Rev. B* **95**, 115433 (2017).
- [48] G. A. Fiete, Colloquium: The spin-incoherent luttinger liquid, *Rev. Mod. Phys.* **79**, 801 (2007).
- [49] As the relevant length scale is provided by the quartic part of the double well potential, here, we consider a modification of the standard  $r_s$  parameter as originally introduced by Wigner, implemented to the situation we investigate.
- [50] M. Ciafaloni and C. Destri, Effective potential and asymmetric instantons, *Nuovo Cim. A* **99**, 449 (1988).
- [51] T. Grafke, R. Grauer, and T. Schäfer, The instanton method and its numerical implementation in fluid mechanics, *Journal of Physics A: Mathematical and Theoretical* **48**, 333001 (2015).
- [52] J. O. Richardson, Ring-polymer instanton theory, *International Reviews in Physical Chemistry* **37**, 171 (2018).
- [53] D. Vanderbilt and S. G. Louie, A monte carlo simulated annealing approach to optimization over continuous variables, *Journal of Computational Physics* **56**, 259 (1984).
- [54] R. MacKenzie, Path integral methods and applications (2000), [arXiv:quant-ph/0004090](https://arxiv.org/abs/quant-ph/0004090) [quant-ph].
- [55] S. R. White, Density matrix formulation for quantum renormalization groups, *Phys. Rev. Lett.* **69**, 2863 (1992).
- [56] U. Schollwöck, The density-matrix renormalization group, *Rev. Mod. Phys.* **77**, 259 (2005).
- [57] U. Schollwöck, The density-matrix renormalization group in the age of matrix product states, *Annals of Physics* **326**, 96 (2011), january 2011 Special Issue.
- [58] I. P. McCulloch, From density-matrix renormalization group to matrix product states, *Journal of Statistical Mechanics: Theory and Experiment* **2007**, P10014 (2007).
- [59] Ö. Legeza and J. Sólyom, Optimizing the density-matrix renormalization group method using quantum information entropy, *Phys. Rev. B* **68**, 195116 (2003).
- [60] Ö. Legeza and G. Fáth, Accuracy of the density-matrix renormalization-group method, *Physical Review B* **53**, 14349 (1996).
- [61] I. Hagymási and O. Legeza, Entanglement, excitations, and correlation effects in narrow zigzag graphene nanoribbons, *Phys. Rev. B* **94**, 165147 (2016).
- [62] H. D. Simon, Analysis of the symmetric lanczos algorithm with reorthogonalization methods, *Linear Algebra and its Applications* **61**, 101 (1984).
- [63] E. A. Laird, F. Kuemmeth, G. A. Steele, K. Grove-Rasmussen, J. Nygård, K. Flensberg, and L. P. Kouwenhoven, Quantum transport in carbon nanotubes, *Rev. Mod. Phys.* **87**, 703 (2015).
- [64] P. W. Anderson, Infrared catastrophe in fermi gases with local scattering potentials, *Phys. Rev. Lett.* **18**, 1049 (1967).
- [65] A. J. Leggett, S. Chakravarty, A. T. Dorsey, M. P. A. Fisher, A. Garg, and W. Zwerger, Dynamics of the dissipative two-state system, *Rev. Mod. Phys.* **59**, 1 (1987).
- [66] L. I. Glazman, I. M. Ruzin, and B. I. Shklovskii, Quantum transport and pinning of a one-dimensional wigner crystal, *Phys. Rev. B* **45**, 8454 (1992).
- [67] C. L. Kane and M. P. A. Fisher, Transmission through barriers and resonant tunneling in an interacting one-dimensional electron gas, *Phys. Rev. B* **46**, 15233 (1992).
- [68] J. Jang, B. M. Hunt, L. N. Pfeiffer, K. W. West, and R. C. Ashoori, Sharp tunnelling resonance from the vibrations of an electronic wigner crystal, *Nature Physics* **13**, 340–344

- (2016).
- [69] H. Zhou, H. Polshyn, T. Taniguchi, K. Watanabe, and A. F. Young, Solids of quantum hall skyrmions in graphene, *Nature Physics* **16**, 154–158 (2019).
- [70] G. A. Fiete and L. Balents, Green’s function for magnetically incoherent interacting electrons in one dimension, *Phys. Rev. Lett.* **93**, 226401 (2004).